


## Article

# Development and Application of High-Internal-Phase Water-in-Oil Emulsions Using Amphiphilic Nanoparticle-Based Emulsifiers

Chunhua Zhao <sup>1,2</sup>, Xiujun Wang <sup>1,2</sup>, Jian Zhang <sup>1,2</sup>, Yigang Liu <sup>1,3</sup>, Changlong Liu <sup>1,3</sup>, Bo Huang <sup>1,2</sup> and Yang Yang <sup>4,\*</sup> 

- <sup>1</sup> State Key Laboratory of Offshore Oil and Gas Exploitation, Beijing 100027, China; zhaochh16@cnooc.com.cn (C.Z.); wangxj89@cnooc.com.cn (X.W.); zhangjian@cnooc.com.cn (J.Z.); liuyg@cnooc.com.cn (Y.L.); liuchl7@cnooc.com.cn (C.L.); huangbo@cnooc.com.cn (B.H.)  
<sup>2</sup> CNOOC Research Institute Ltd., Beijing 100027, China  
<sup>3</sup> Tianjin Branch of CNOOC Ltd., Tianjin 300452, China  
<sup>4</sup> College of Energy, Chengdu University of Technology, Chengdu 610059, China  
\* Correspondence: yangyang19@cdut.edu.cn

**Abstract:** High-internal-phase water-in-oil (W/O) emulsions generated in situ have garnered considerable attention as novel profile control systems. However, conventional emulsifiers are unreactive and poorly dispersed in water, necessitating large dosages and resulting in poor injectivity. In this study, we synthesized amphiphilic nanoparticles (SiO<sub>2</sub>-NH<sub>2</sub>-DAC NPs) containing amine and long-chain alkyl groups using a one-pot method and investigated the stabilized emulsion properties. Our results indicated that W/O emulsions with a water-to-oil ratio (WOR) of 7:3 to 8:2 could be prepared with just 0.1 wt% of SiO<sub>2</sub>-NH<sub>2</sub>-DAC NPs under neutral and basic conditions, with demulsification occurring under acidic conditions (pH = 2.1), demonstrating the pH-responsiveness of the W/O emulsions. The emulsion viscosity increased from 150 to 2555 mPa·s at different WORs. An additional 18.7% oil recovery was achieved using SiO<sub>2</sub>-NH<sub>2</sub>-DAC NPs in a heterogeneous core, highlighting their potential as a promising profile control candidate.

**Keywords:** W/O emulsions; pH responsiveness; amphiphilicity; nanoparticles



**Citation:** Zhao, C.; Wang, X.; Zhang, J.; Liu, Y.; Liu, C.; Huang, B.; Yang, Y. Development and Application of High-Internal-Phase Water-in-Oil Emulsions Using Amphiphilic Nanoparticle-Based Emulsifiers. *Polymers* **2024**, *16*, 3148. <https://doi.org/10.3390/polym16223148>

Academic Editors: Gregory T. Russell and Eduardo Guzmán

Received: 29 September 2024  
Revised: 1 November 2024  
Accepted: 11 November 2024  
Published: 12 November 2024



**Copyright:** © 2024 by the authors. Licensee MDPI, Basel, Switzerland. This article is an open access article distributed under the terms and conditions of the Creative Commons Attribution (CC BY) license (<https://creativecommons.org/licenses/by/4.0/>).

## 1. Introduction

Prolonged water injection in oilfields leads to water channeling, high water content, and severe ineffective circulation [1,2]. In water-swept regions, residual oil saturation is low [3], while unswept areas hold substantial unrecovered crude oil [4,5]. Therefore, profile control techniques are essential to boost the water injection efficiency and enhance oil recovery [6].

Current profile control techniques encompass chemical profile control [7], mechanical profile control, foam profile control [8], microbial profile control [9], and oily sludge profile control [10,11]. Mechanical profile control only addresses water injection issues near the wellbore area [12]. Foam profile control is characterized by high temperature and salt resistance [13], a high resistance coefficient, and a low residual resistance coefficient, but its foaming capacity and stability are significantly influenced by formation conditions [14]. Microbial profile control is highly selective in oil environments but poses a high risk of blockage near the well zone. Chemical profile control allows the selection of polymer gels [15], particles [16,17], microspheres [18], and other systems to suit diverse reservoir conditions [19,20].

The recently developed in situ emulsification profile control technology for crude oil exploits residual oil to create high-internal-phase water-in-oil emulsions (W/O HIPes) in water-swept areas [21–25], thereby increasing flow resistance and directing subsequent water injections into middle- and low-permeability layers. W/O HIPes, with oil as the

continuous phase and water as the dispersed phase, have an aqueous-phase system fraction exceeding 74% [26]. The emulsion droplets compress and deform, forming a highly viscous fluid [27,28]. Emulsifiers capable of forming W/O emulsions include the Span series [28,29], polyglyceride fatty acid esters, and lecithin [30–33]. However, these emulsifiers exhibit low hydrophile–lipophile balance values and strong hydrophobicity [34], resulting in their poor dispersion in water. Crude oil often contains acidic components [35,36], which can react with alkalis to form fatty acid soaps at the interface, stabilizing it [37]. However, emulsifiers without reactive groups struggle to synergize with these acidic components, necessitating high emulsifier doses. This challenge complicates demulsification and oil–water separation, increasing the risk of reservoir plugging. Recently, responsive Pickering emulsions have garnered research interest [38–40]. Modifying nanoparticles (NPs) with responsive groups can enhance mobility control and facilitate blockage removal via demulsification, particularly under pH-responsiveness. Amines and their derivatives, highly reactive to acids, enable functional NPs to act as pH-responsive switches, altering emulsion types through amine protonation [41].

In this study, we synthesized amine-modified NPs from tetraethyl orthosilicate and 3-aminopropyl triethoxysilane using a one-pot method. Additionally, amphiphilic NPs ( $\text{SiO}_2\text{-NH}_2\text{-DAC}$  NPs) were created by introducing hydrophobic units via a substitution reaction between acyl chloride and amine groups. These NPs served as emulsifiers to prepare stable W/O emulsions. The basicity of the amine groups on the NP surface enables rapid conversion of the emulsion types and reduces the NP concentration. Our findings suggest that these NPs are highly valuable for enhancing mobility control and demulsification for blockage removal.

## 2. Experimental Section

### 2.1. Materials

Tetraethyl orthosilicate (TEOS, 98%), 3-aminopropyl triethoxysilane (APTES, 99%), dodecanoyl chloride (DAC, 98%),  $\text{NH}_3\cdot\text{H}_2\text{O}$  (25–28%), NaCl (99.5%),  $\text{CaCl}_2$  (96%), and  $\text{NaHCO}_3$  (99.8%) were purchased from Aladdin Chemical Reagent Company. The parameters of the used crude oil and simulated water are listed in Tables 1 and 2, respectively.

**Table 1.** The parameters of the used crude oil.

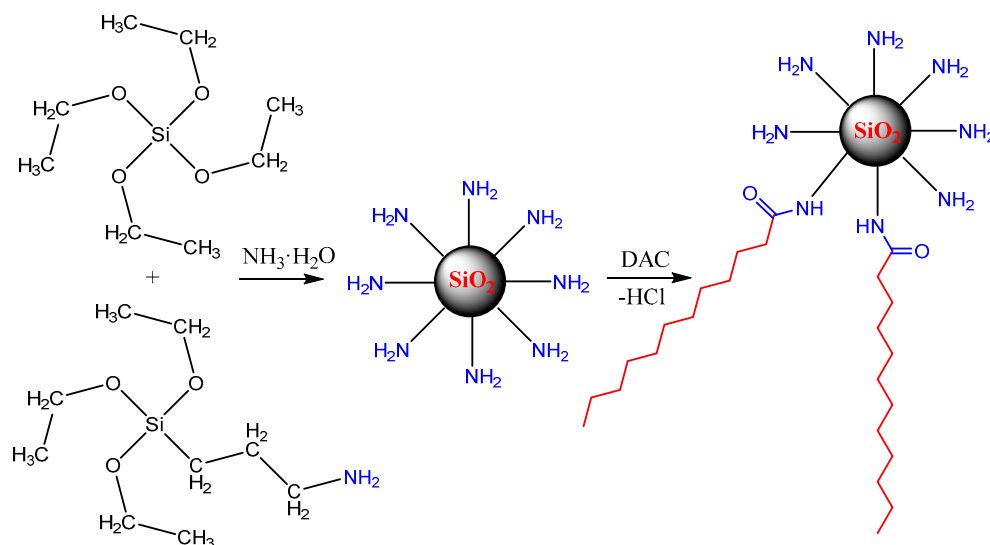
Density ( $\text{g}/\text{cm}^3$ )	Acid Value ( $\text{mg KOH}/\text{g}$ )	Viscosity ( $\text{mPa}\cdot\text{s}$ )
0.917	3.1	151

**Table 2.** The parameters of the simulated water.

$\text{Na}^+$ ( $\text{mg}/\text{L}$ )	$\text{K}^+$ ( $\text{mg}/\text{L}$ )	$\text{Ca}^{2+}$ ( $\text{mg}/\text{L}$ )	$\text{Mg}^{2+}$ ( $\text{mg}/\text{L}$ )	$\text{Cl}^-$ ( $\text{mg}/\text{L}$ )	$\text{HCO}_3^-$ ( $\text{mg}/\text{L}$ )	$\text{SO}_4^{2-}$ ( $\text{mg}/\text{L}$ )	Salinity ( $\text{mg}/\text{L}$ )
10,052.08	105.96	366.88	1172.08	17,588.09	153.25	2691	32,129.33

### 2.2. Synthesis of $\text{SiO}_2\text{-NH}_2\text{-DAC}$ NPs

$\text{SiO}_2\text{-NH}_2$  NPs were synthesized by a modified Stöber method (Scheme 1). Generally, 2 mL of TEOS was added to a solution containing 40 mL of ethanol, 3 mL of deionized water, and 0.8 mL of  $\text{NH}_3\cdot\text{H}_2\text{O}$ . The mixture was stirred at 45 °C for 12 h. Afterwards, 2 mL of APTES was added to the mixture to functionalize the surface with amino groups. Then, 0.5 mL of DAC was added dropwise to the mixture at 0 °C. After reaction for 6 h, the mixture was centrifuged and washed with ethanol to obtain a white powder ( $\text{SiO}_2\text{-NH}_2\text{-DAC}$  NPs).



**Scheme 1.** The synthesis route of SiO<sub>2</sub>-NH<sub>2</sub>-DAC NPs.

### 2.3. Structure Characterization

The products were dried in a vacuum oven at 80 °C to constant weight, after mixing a small amount of the samples with KBr, pressing the powder into pellets, and determining the infrared spectrum (Nicolet 6700, Thermo Fisher Scientific, Waltham, MA, USA) in the wavenumber range of 4000–500 cm<sup>-1</sup>. A thermogravimetric analyzer (STA8000, PerkinElmer, Waltham, MA, USA) was used to study the thermal stability of the samples under the test conditions: nitrogen atmosphere, temperature range of 30–800 °C, and heating rate of 10 °C/min. The surface composition of the nanoparticles was determined by X-ray photoelectron spectroscopy (Thermo Kalpha, Thermo Fisher Scientific, USA). The sample was pressed on a glass slide, and the contact angle of the sample was determined by the SL200KS optical contact goniometer at room temperature. The pH of the particle dispersion was adjusted to a specific value at a concentration of 0.01% by mass, and the particle size and zeta potential of the dispersion were determined by a Malvern Zetasizer (Nano ZS90, Malvern, UK). The X-ray diffraction pattern of the sample was determined using a ray diffractometer (D/MAX-RB, Rigaku, Tokyo, Japan) with a scanning angle of 10°–80° and a scanning speed of 10°/min. The dried powder of the sample was dispersed in ethanol and sonicated for 30 min, and then the samples were dropped on a conductive adhesive and their surface morphology was observed by SEM. The dynamic interfacial tension (IFT) between the heavy oil and the different systems was measured by an interfacial tensiometer (SDT, CRUSS, Hamburg, Germany) at 6000 rpm and 90 °C. The IFT value was recorded every 30 s.

### 2.4. Preparation and Evaluation of the Emulsions

The designed amount of SiO<sub>2</sub>-NH<sub>2</sub>-DAC NPs was dispersed in saline water. Then, the crude oil was added to the dispersion. Water-to-oil volume ratios (WORs) of 7:3, 7.5:2.5, and 8:2 were used. The mixture was stirred at 400 r/min for 1 h. An oil bath was used to control the temperature (90 °C). The prepared emulsions were transferred to colorimetric tubes. The tubes were preheated to the specified temperature in an oven. Then, the dewatering volume ( $V_d$ ) was recorded at different times. The dewatering rate ( $R_d$ ) was calculated to evaluate the stability of the emulsions.  $V_t$  was the volume of the used dispersion.

$$R_d = \frac{V_d}{V_t} \times 100\%$$

The viscosity of the prepared emulsions was determined using a Brookfield DV2T viscometer (64# spindle, 34 r/min) with a shear rate of 7.34 s<sup>-1</sup>. The rheological curves of

the prepared polymer solution were plotted using a rheometer (Malvern Kinexus, Malvern, UK). In rheological experiments, the frequency sweep curve was plotted at frequencies ranging from 0.1 to 10 Hz using a rheometer (MCR 302, Anton Paar, Graz, Austria) and CP50-1-SN30644 (Anton Paar, Austria) plate clamps (diameter = 0.099 mm). The micrographs of the prepared emulsions were measured by an optical microscope (CX40, Sunny Optical Technology Company, Ningbo, China) at room temperature.

### 2.5. Oil Displacement Ability in Heterogeneous Core

A two-layer heterogeneous sandstone core (permeability 200/600 mD, determined by perm-plug method; Figure 1) with a cuboid shape (4.5 cm × 4.5 cm × 30 cm) was saturated with crude oil (porosity 23.4%, oil saturation 66.5%). The core was placed in the core holder with the casing pressure at 30 °C. Then, water flooding was conducted at a constant injection flow rate of 0.3 mL/min. After that, a 0.3 PV nanoparticle slug was injected when the water cut reached 80%. Finally, water flooding was conducted continually until the economic limit (98%) was reached. The pressure and enhanced oil recovery (EOR) value were recorded.

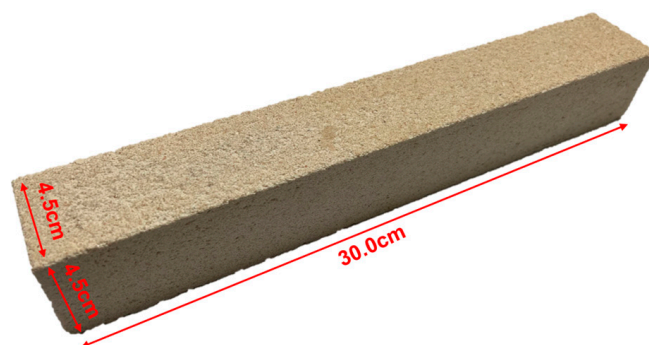


Figure 1. Heterogeneous core used in core flooding experiment.

## 3. Results and Discussion

### 3.1. Results of Structural Characterization

In Figure 2a, the peak at 3330–3359  $\text{cm}^{-1}$  corresponds to the  $-\text{NH}_2$  group, while the peaks at 2856 and 2925  $\text{cm}^{-1}$  correspond to the  $-\text{CH}_2-$  group. The  $-\text{OH}$  peak of silica disappeared, confirming an adequate reaction between silica and the amine group. Additionally, in the  $\text{SiO}_2-\text{NH}_2-\text{DAC}$  spectrum, the  $\text{N}-\text{H}$  stretching peak in the amide group appeared at 3286  $\text{cm}^{-1}$ , and the  $-\text{C}=\text{O}$  vibration peak appeared at 1645  $\text{cm}^{-1}$ , indicating that DAC reacts with the amine group to form an amide bond. These results confirm the successful introduction of amine groups and hydrophobic units onto the silica surface.

The X-ray diffraction patterns (Figure 2b) displayed a characteristic peak at  $21.5^\circ$ , confirming the product as amorphous silica. X-ray photoelectron spectroscopy (Figure 2c) revealed the presence of silicon (7.31%), carbon (67.4%), nitrogen (6.86%), and oxygen (18.43%). The thermogravimetric analysis (Figure 2d) indicated weight loss below 200 °C, owing to crystalline water in the amphiphilic NPs, and between 380 and 550 °C, caused by the decomposition of the organic carbon chain. Beyond 800 °C, the weight stabilized at 35%, indicating significant organic content on the NPs' surface. The critical micelle concentration (CMC) was about 0.09% (Figure 2e). Scanning electron microscopy (Figure 2f) showed that the  $\text{SiO}_2-\text{NH}_2-\text{DAC}$  NPs were spherical, averaging 100 nm in size.

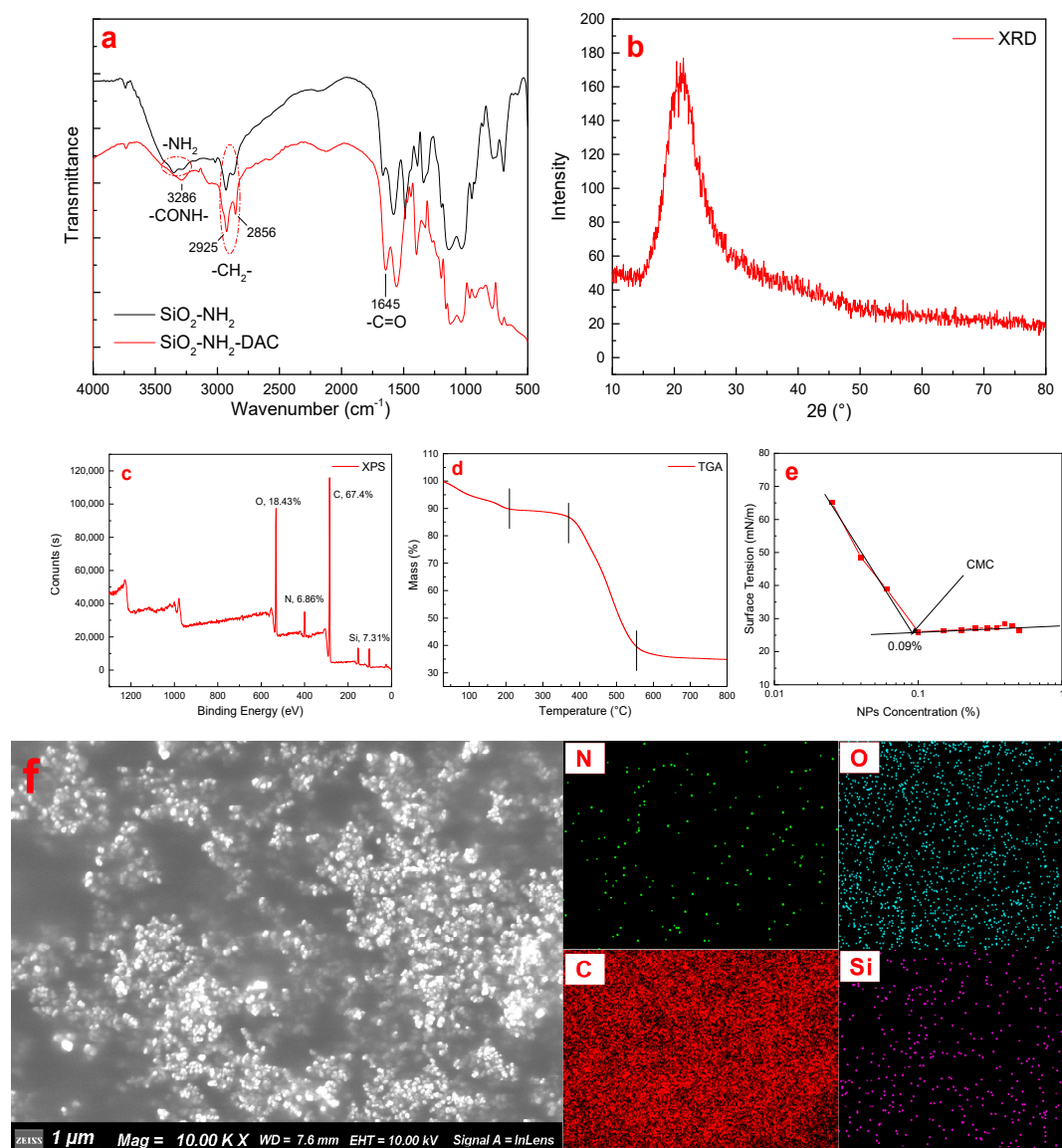


**Figure 2.** The structural characterization of  $\text{SiO}_2\text{-NH}_2\text{-DAC}$ : (a) FTIR spectra, (b) XRD spectrum, (c) XPS spectrum, (d) TGA curve, (e) surface tension curve, (f) SEM and mapping images.

### 3.2. Emulsifying Capacity of $\text{SiO}_2\text{-NH}_2\text{-DAC}$ NPs

The surface of  $\text{SiO}_2\text{-NH}_2\text{-DAC}$  NPs features amine groups and long carbon chains, making it amphiphilic and aiding in emulsion formation. At high WOR, emulsion droplets are compressed and deformed, creating a high-viscosity fluid. As shown in Figure 3a, the viscosity sharply increased to 1520 mPa·s at an NP concentration of 0.1%, significantly higher than the crude oil's viscosity, indicating thorough emulsification and suggesting effective mobility control; this result is corroborated by the photographs shown in Figure 3b. NPs spontaneously aggregate at the two-phase interface, forming an interfacial membrane [42]. The membrane's strength increases with increasing NP concentration; thus, when the NP concentration exceeds 0.1%, the emulsion viscosity continues to increase. The interfacial membrane also prevents emulsion droplet coalescence, stabilizing the emulsion [43,44]. Consequently, the  $R_d$  value decreased markedly, showing good emulsion stability (Figure 3c).

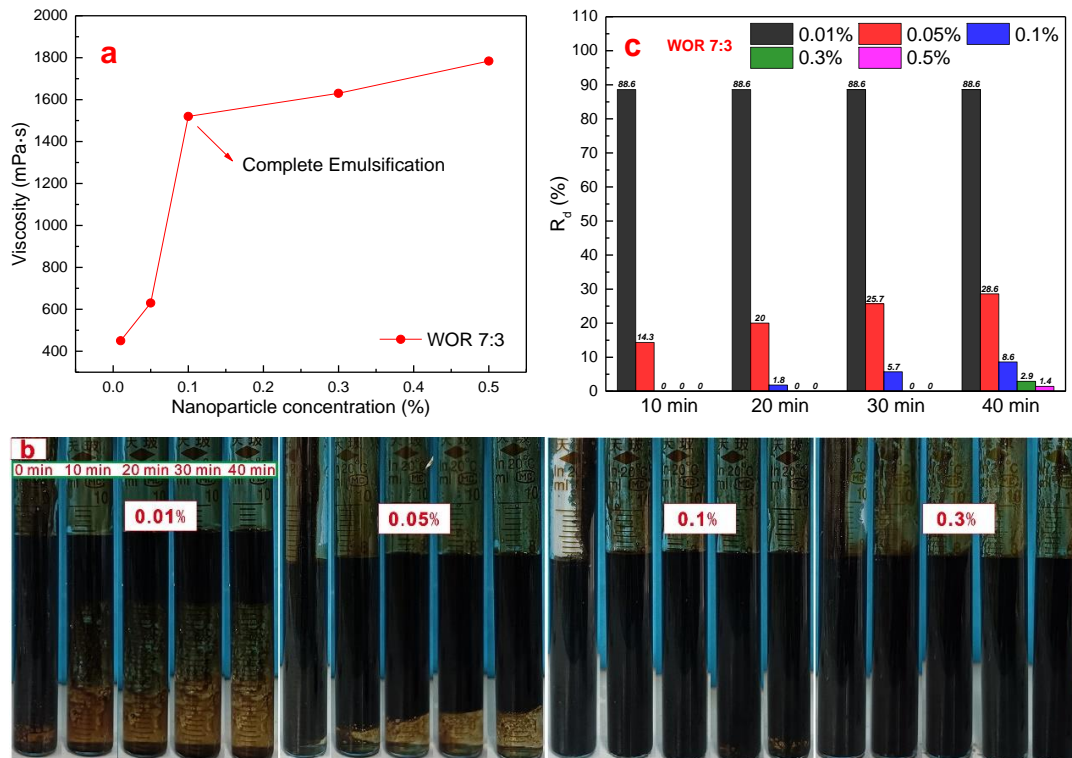


**Figure 3.** The emulsion properties of SiO<sub>2</sub>–NH<sub>2</sub>–DAC NPs at different concentrations: (a) the influence of nanoparticle concentration on the viscosity of the emulsions; (b) the photographs of the emulsions; (c) the dewatering rate at different times.

During water flooding, the water–oil ratio (WOR) increases in water-swept areas, particularly in medium- and high-permeability layers, reducing residual oil saturation and flow resistance, and causing an ineffective water injection cycle. In this study, three WORs were used. Figure 4a,b reveal that as the WOR increased, the viscosity and viscous modulus increased rapidly owing to the compression and deformation of emulsion droplets. Additionally, NPs aggregated at the oil–water interface, forming an elastic interface membrane, making the elastic modulus significantly higher than the viscous modulus. However, the emulsion stability decreased with increasing R<sub>d</sub> value at a high WOR (Figure 4c). Studies suggest that NPs can stabilize emulsions with surfactants [45–47]. Thus, to increase the WOR, the NP dosage can be increased, or a small amount of emulsifier can be added.

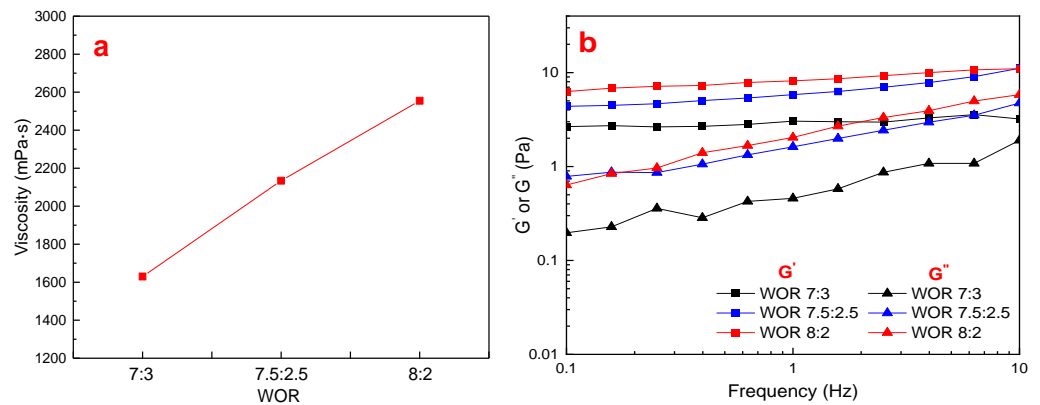


**Figure 4.** Cont.

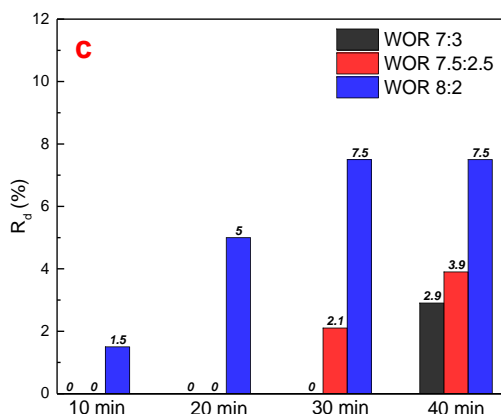
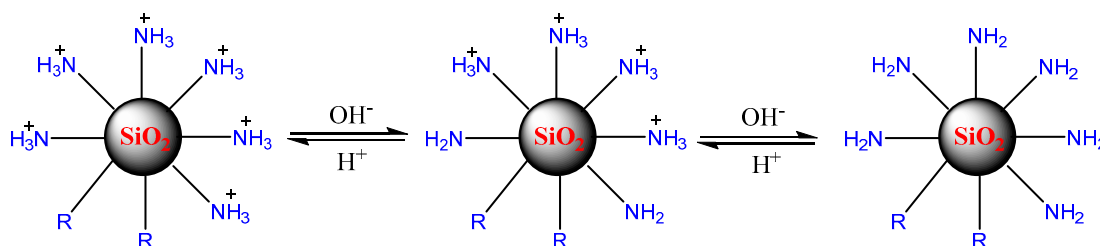


**Figure 4.** The emulsion properties of SiO<sub>2</sub>-NH<sub>2</sub>-DAC NPs (0.3%) at different WORs: (a) the influence of WOR on the viscosity of the emulsions; (b) the viscoelasticity of the emulsions; (c) the dewatering rate at different times.

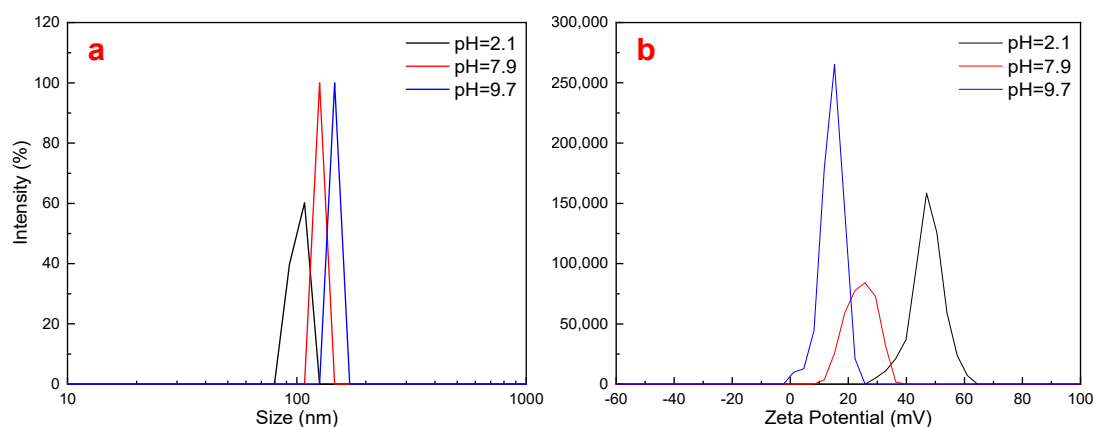
### 3.3. pH Sensitivity of SiO<sub>2</sub>-NH<sub>2</sub>-DAC NPs

The SiO<sub>2</sub>-NH<sub>2</sub>-DAC NPs' surface contains two characteristic units: an amine group and a long-chain alkyl group. The amine group imparts pH-responsiveness to the NPs (Scheme 2).



**Scheme 2.** The pH-responsiveness of SiO<sub>2</sub>-NH<sub>2</sub>-DAC NPs.

Upon protonating the amine group, the NPs showed increased surface charge and a significantly elevated positive zeta potential (Table 3 and Figure 5). This electrostatic repulsion reduced the binding forces between NPs, enhancing their dispersity and decreasing their size to 29.9 nm under acidic conditions. As the pH increased, protonation decreased, leading to a lower zeta potential. Consequently, the repulsive forces weakened, causing an increase in the NPs' size. These findings demonstrate a positive correlation between zeta potential and NP dispersibility, with a higher zeta potential leading to better dispersibility.

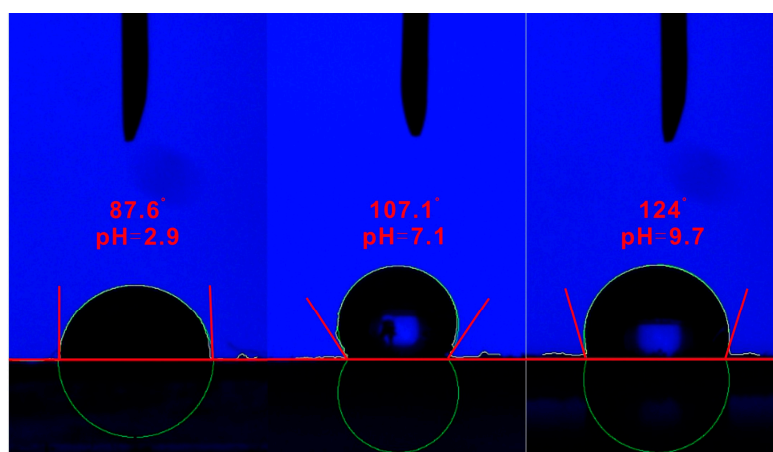


**Figure 5.** The influence of pH on the (a) size and (b) zeta potential of SiO<sub>2</sub>-NH<sub>2</sub>-DAC.

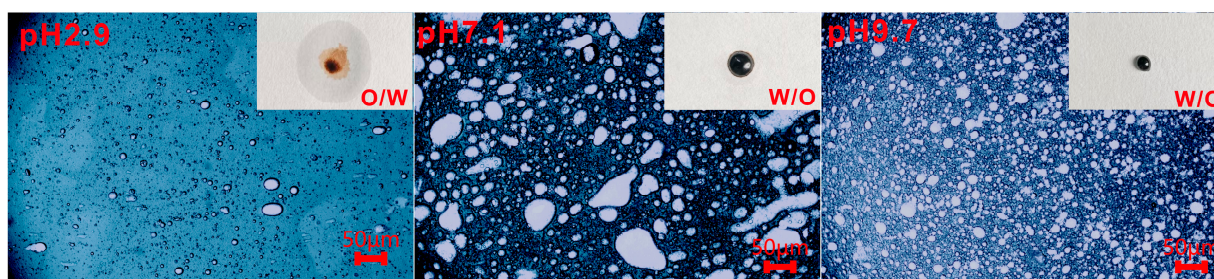
**Table 3.** The size and zeta potential of SiO<sub>2</sub>-NH<sub>2</sub>-DAC at different pH.

pH	2.9	7.1	9.7
Average Size (nm)	29.9	125.6	146.1
Zeta Potential (mV)	47.21	23.01	12.43

The pH-responsiveness of SiO<sub>2</sub>-NH<sub>2</sub>-DAC NPs is evident from the contact angle measurements. As shown in Figure 6, under alkaline conditions, the weak hydrophilicity of the amine groups and strong hydrophobicity of the alkyl chains yielded a contact angle of 124°. As the pH decreased, the amine groups converted into hydrophilic amine salts, reducing the contact angle to 107.1° and 87.6° at pH = 7.1 and 2.9, respectively.

**Figure 6.** The contact angle at different pH.

NPs with amphiphilic properties, such as surfactants, rapidly aggregate at the two-phase interface, thereby stabilizing it. Hydrophobic emulsifiers are used for W/O emulsions, while hydrophilic emulsifiers prepare oil-in-water (O/W) emulsions [48]. Utilizing the pH-responsiveness of SiO<sub>2</sub>-NH<sub>2</sub>-DAC NPs, we aimed to control emulsion types by adjusting the amine group's protonation state. As illustrated in Figure 7, the NPs were hydrophobic, forming a W/O emulsion, but under acidic conditions their hydrophilicity increased, forming an O/W emulsion. This change in emulsion type can enhance mobility control and blockage removal.

**Figure 7.** The micrographs of the emulsions at different pH.

The amine group, an alkaline functional group, reacts with the acidic components in crude oil to form fatty acid soaps at the two-phase interface, thereby stabilizing it. Figure 8a shows that interfacial tension (IFT) is strongly influenced by the protonation of the amine group on NP surfaces. The amine group's ability to generate surfactants in situ is crucial for SiO<sub>2</sub>-NH<sub>2</sub>-DAC to stabilize emulsions at low concentrations. In contrast, stable W/O emulsions cannot be created using hydrophobic or hydrophilic SiO<sub>2</sub> (Figure 8b). Increased



protonation of the amine group reduces its reactivity with acidic components, increasing the interfacial tension under neutral conditions. Full protonation forms an amine salt with a long-chain alkyl group, producing a giant cationic surfactant that effectively reduces interfacial tension.

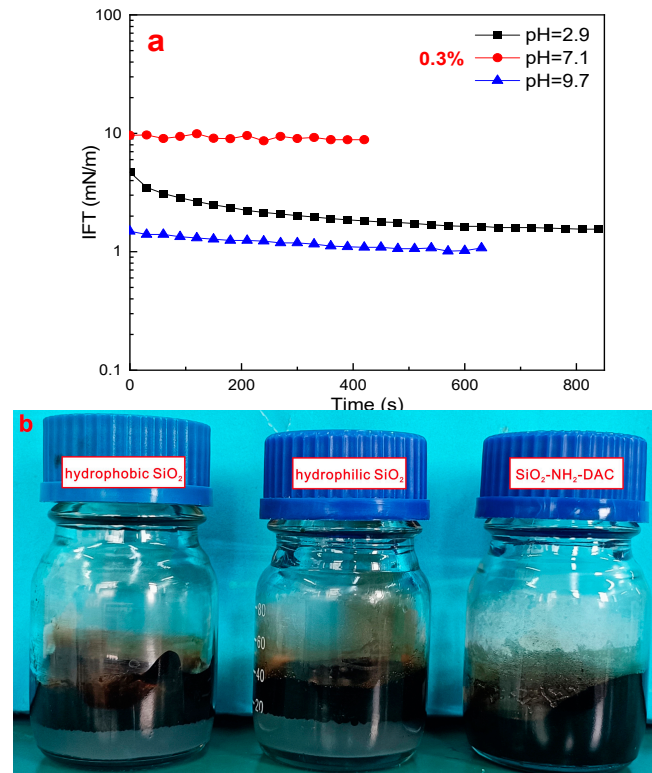


**Figure 8.** (a) The influence of pH on the IFT, and (b) the emulsion photographs of different nanoparticles.

### 3.4. Core Flooding Experiments of SiO<sub>2</sub>-NH<sub>2</sub>-DAC NPs

Due to the core's heterogeneity, only 23.8% oil recovery was achieved by the end of water flooding (Figure 9). Injection of 0.3 PV SiO<sub>2</sub>-NH<sub>2</sub>-DAC NPs gradually increased the injection pressure to 0.66 MPa, with notable fluctuations in the subsequent water flooding stage. This pressure increase can be attributed to an increase in the displacement resistance caused by the in situ HIPE formation. Unlike polymer gels, emulsion drops are flexible, leading to dynamic capture and re-migration characteristics that cause pressure fluctuations. As HIPE formation is time-consuming, the pressure increase was delayed until after the injection of 0.2 PV SiO<sub>2</sub>-NH<sub>2</sub>-DAC NPs. The oil recovery improved owing to the profile control effect of the HIPEs formed in situ, which enhanced the sweep efficiency by migrating the flooding phase into the core's low-permeability areas. Consequently, oil recovery rose to 42.5% after subsequent water flooding, achieving an additional 18.7% oil recovery with SiO<sub>2</sub>-NH<sub>2</sub>-DAC NPs. In comparison, the enhanced oil recovery of hydrophilic SiO<sub>2</sub> was only 7.3%, which is much lower than that of the SiO<sub>2</sub>-NH<sub>2</sub>-DAC NPs. The results demonstrate the potential of SiO<sub>2</sub>-NH<sub>2</sub>-DAC NPs as a profile control agent for enhanced oil recovery.

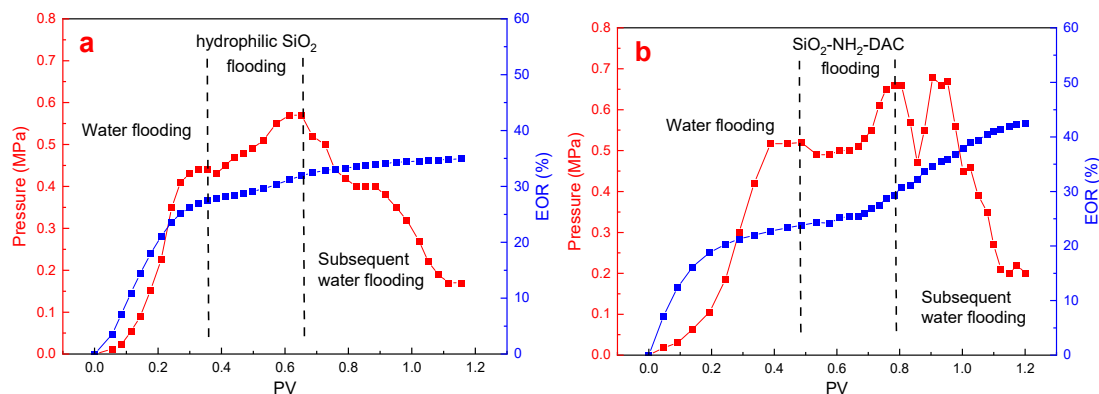


Figure 9. The displacement results of hydrophilic SiO<sub>2</sub> (a) and SiO<sub>2</sub>-NH<sub>2</sub>-DAC NPs (b).

#### 4. Conclusions

In this study, amine-modified NPs were synthesized from tetraethyl orthosilicate and 3-aminopropyl triethoxysilane using a one-pot method, and amphiphilic NPs (SiO<sub>2</sub>-NH<sub>2</sub>-DAC NPs) were prepared by introducing hydrophobic units via a substitution reaction between acyl chloride and amine groups. SiO<sub>2</sub>-NH<sub>2</sub>-DAC NPs, featuring amine and long-chain alkyl groups with amphiphilic properties, served as emulsifiers for W/O HIPEs up to a WOR of 8:2. The pH-responsive amine groups altered the contact angle from hydrophobic to hydrophilic, converting the emulsion type from W/O to O/W. These alkaline amine groups also reacted with acidic crude oil components, reducing the NP dosage. A concentration of 0.1% was found to be sufficient to form HIPEs effectively. HIPE formation in the core was validated by the observed increase and fluctuations in pressure during displacement. The SiO<sub>2</sub>-NH<sub>2</sub>-DAC NPs achieved an additional 18.7% oil recovery, demonstrating significant potential for profile control.

**Author Contributions:** Methodology, X.W.; formal analysis, B.H.; investigation, Y.L. and Y.Y.; writing—original draft, C.Z.; writing—review and editing, Y.Y.; supervision, J.Z. and C.L.; funding acquisition, Y.Y. All authors have read and agreed to the published version of the manuscript.

**Funding:** This work was supported by the National Natural Science Foundation of China (U22B6005), the Key Technologies R&D Program of CNOOC (KJGG2021-0504), the Technologies Program of CNOOC Research Institute Ltd. (2023-GX-14), the National Natural Science Foundation of China (No. 52204028), and the Natural Science Foundation of Sichuan Province (No. 2023NSFSC0942).

**Institutional Review Board Statement:** Not applicable.

**Data Availability Statement:** The original contributions presented in this study are included in the article; further inquiries can be directed to the corresponding author.

**Conflicts of Interest:** C.Z., X.W., J.Z., Y.L., C.L. and B.H. were employed by the company China National Offshore Oil Corporation (China). The remaining authors declare that this research was conducted in the absence of any commercial or financial relationships that could be construed as potential conflicts of interest.

#### References

- Lin, Y.-B.; Zhang, J.; Liu, X.-G.; Zhou, H.-T. Pore structure features of reservoirs at late high water-cut stage, Lamadian Oilfield, Daqing, China. *Pet. Explor. Dev.* **2008**, *35*, 215–219. [[CrossRef](#)]
- Sun, K.; Liu, H.; Wang, Y.; Ge, L.; Gao, J.; Du, W. Novel Method for Inverted Five-Spot Reservoir Simulation at High Water-Cut Stage Based on Time-Varying Relative Permeability Curves. *ACS Omega* **2020**, *5*, 13312–13323. [[CrossRef](#)] [[PubMed](#)]
- Zivar, D.; Pourafshary, P.; Moradpour, N. Capillary desaturation curve: Does low salinity surfactant flooding significantly reduce the residual oil saturation? *J. Pet. Explor. Prod.* **2021**, *11*, 783–794. [[CrossRef](#)]
- Sang, Q.; Li, Y.; Yu, L.; Li, Z.; Dong, M. Enhanced oil recovery by branched-preformed particle gel injection in parallel-sandpack models. *Fuel* **2014**, *136*, 295–306. [[CrossRef](#)]
- Zhu, D.; Hou, J.; Chen, Y.; Zhao, S.; Bai, B. In Situ Surface Decorated Polymer Microsphere Technology for Enhanced Oil Recovery in High-Temperature Petroleum Reservoirs. *Energy Fuels* **2018**, *32*, 3312–3321. [[CrossRef](#)]

6. Liu, J.; Li, L.; Xu, Z.; Sun, Y.; Wu, Y.; Dai, C. Biomimetic functional hydrogel particles with enhanced adhesion characteristics for applications in fracture conformance control. *J. Ind. Eng. Chem.* **2022**, *106*, 482–491. [[CrossRef](#)]
7. Dai, C.; Qing, Y.; Qilin, G.; Fulin, Z. Study and Application of In-depth Water Control Technology for Production Wells. *Pet. Sci. Technol.* **2011**, *29*, 2568–2577. [[CrossRef](#)]
8. Seddiqi, K.N.; Abe, K.; Hao, H.; Mahdi, Z.; Liu, H.; Hou, J. Optimization and Performance Evaluation of a Foam Plugging Profile Control Well Selection System. *ACS Omega* **2023**, *8*, 10342–10354. [[CrossRef](#)]
9. Bi, Y.Q.; Yu, L.; Huang, L.X.; Ma, T.; Xiu, J.L.; Yi, L.N. Microscopic profile control mechanism and potential application of the biopolymer-producing strain FY-07 for microbial enhanced oil recovery. *Pet. Sci. Technol.* **2016**, *34*, 1952–1957. [[CrossRef](#)]
10. Caili, D.; Qing, Y.; Fulin, Z. In-depth Profile Control Technologies in China—A Review of the State of the Art. *Pet. Sci. Technol.* **2010**, *28*, 1307–1315. [[CrossRef](#)]
11. Lv, B.; Sun, P.; Wu, Y.; Yang, Z.; Liu, P.; Wang, C.; Liu, Q. Study and Application of Oily Sludge Profile Control Technology in Heavy Oil Reservoir. *Energies* **2023**, *16*, 5064. [[CrossRef](#)]
12. Wei, J.; Zhou, X.; Zhang, D.; Li, J. Laboratory Experimental Optimization of Gel Flooding Parameters to Enhance Oil Recovery during Field Applications. *ACS Omega* **2021**, *6*, 14968–14976. [[CrossRef](#)] [[PubMed](#)]
13. Yang, L.-L.; He, X.-B.; Cheng, Y.-X.; Jiang, G.-C.; Liu, Z.-Y.; Wang, S.-B.; Qiu, S.-X.; Wang, J.-H.; Tian, W.-G. Eco-friendly aqueous foam stabilized by cellulose microfibrils with great salt tolerance and high temperature resistance. *Pet. Sci.* **2023**, *20*, 2499–2511. [[CrossRef](#)]
14. Wei, P.; Pu, W.; Sun, L.; Wang, B. Research on nitrogen foam for enhancing oil recovery in harsh reservoirs. *J. Pet. Sci. Eng.* **2017**, *157*, 27–38. [[CrossRef](#)]
15. Gong, H.; Zhang, H.; Xu, L.; Li, K.; Yu, L.; San, Q.; Li, Y.; Dong, M. The Synergistic Effect of Branched-Preformed Particle Gel and Hydrolyzed Polyacrylamide on Further-Enhanced Oil Recovery after Polymer Flooding. *Energy Fuels* **2017**, *31*, 7904–7910. [[CrossRef](#)]
16. Rellegadla, S.; Bairwa, H.K.; Kumari, M.R.; Prajapat, G.; Nimesh, S.; Pareek, N.; Jain, S.; Agrawal, A. An Effective Approach for Enhanced Oil Recovery Using Nickel Nanoparticles Assisted Polymer Flooding. *Energy Fuels* **2018**, *32*, 11212–11221. [[CrossRef](#)]
17. Druetta, P.; Picchioni, F. Polymer and nanoparticles flooding as a new method for Enhanced Oil Recovery. *J. Pet. Sci. Eng.* **2019**, *177*, 479–495. [[CrossRef](#)]
18. Zhao, S.; Pu, W. Investigation into the effect of polymer microspheres (PMs) on oil-water relative permeability and oil-in-water emulsion stability for enhanced oil recovery. *J. Dispers. Sci. Technol.* **2020**, *42*, 1695–1702. [[CrossRef](#)]
19. Zou, J.; Yue, X.; Dong, J.; Shao, M.; Wang, L.; Gu, J.; An, W. Novel in-depth profile control agent based on in-situ polymeric microspheres in low permeability reservoir. *J. Dispers. Sci. Technol.* **2020**, *41*, 1254–1264. [[CrossRef](#)]
20. Cao, W.; Xie, K.; Lu, X.; Liu, Y.; Zhang, Y. Effect of profile-control oil-displacement agent on increasing oil recovery and its mechanism. *Fuel* **2019**, *237*, 1151–1160. [[CrossRef](#)]
21. Zhou, Y.; Yin, D.; Li, Y.; He, J.; Zhang, C. A review of crude oil emulsification and multiphase flows in chemical flooding. *Energy Sci. Eng.* **2023**, *11*, 1484–1500. [[CrossRef](#)]
22. Liu, W.; Sun, Z.; Li, N.; Qi, Z.; Wang, Z.; Wang, Z. Binary droplet interactions in shear water-in-oil emulsion: A molecular dynamics study. *J. Mol. Liq.* **2022**, *363*, 119823. [[CrossRef](#)]
23. Pang, S.; Pu, W.; Jiang, F.; Gao, H.; Wang, Y.; Chen, Y.; Wei, P. Effect of water content on features of W/O emulsion during water flooding in heavy oil reservoir: Bulk properties and mobility control characteristics. *J. Pet. Sci. Eng.* **2021**, *207*, 109075. [[CrossRef](#)]
24. Jiang, F.; Gao, D.; Feng, X.; Pan, J.; Pu, W. W/O high internal phase emulsions (HIPEs) stabilized by a piperazinyl based emulsifier. *Soft Matter* **2021**, *17*, 9859–9865. [[CrossRef](#)] [[PubMed](#)]
25. Arab, D.; Kantzas, A.; Bryant, S.L. Nanoparticle stabilized oil in water emulsions: A critical review. *J. Pet. Sci. Eng.* **2018**, *163*, 217–242. [[CrossRef](#)]
26. Masalova, I.; Kharatyan, E.; Tshilumbu, N.N. Effect of the type of the oil phase on stability of highly concentrated water-in-oil emulsions. *Colloid J.* **2013**, *75*, 579–585. [[CrossRef](#)]
27. Sun, X.; Yang, D.; Zhang, H.; Zeng, H.; Tang, T. Unraveling the Interaction of Water-in-Oil Emulsion Droplets via Molecular Simulations and Surface Force Measurements. *J. Phys. Chem. B* **2021**, *125*, 7556–7567. [[CrossRef](#)]
28. Gao, J.; Tong, Z.; Bu, X.; Bilal, M.; Hu, Y.; Ni, C.; Xie, G. Effect of water-in-oil and oil-in-water with Span 80 on coal flotation. *Fuel* **2023**, *337*, 127145. [[CrossRef](#)]
29. Zhao, X.; Tang, Y.; Zhao, B.; Wu, C.; Li, J.; Chu, C.; Liu, K.; Ding, Y. Collecting behaviors of high internal phase (HIP) emulsion in flotation of ultrafine high-ash content coal slime. *Int. J. Coal Prep. Util.* **2022**, *42*, 2635–2655. [[CrossRef](#)]
30. Zembyla, M.; Murray, B.S.; Sarkar, A. Water-in-oil emulsions stabilized by surfactants, biopolymers and/or particles: A review. *Trends Food Sci. Technol.* **2020**, *104*, 49–59. [[CrossRef](#)]
31. Bago Rodriguez, A.M.; Binks, B.P. High internal phase Pickering emulsions. *Curr. Opin. Colloid Interface Sci.* **2022**, *57*, 101556. [[CrossRef](#)]
32. Guan, X.; Ngai, T. pH-Sensitive W/O Pickering High Internal Phase Emulsions and W/O/W High Internal Water-Phase Double Emulsions with Tailored Microstructures Costabilized by Lecithin and Silica Inorganic Particles. *Langmuir* **2021**, *37*, 2843–2854. [[CrossRef](#)] [[PubMed](#)]

33. Mehebab Rahaman, S.; Chakraborty, M.; Mandal, T.; Khatun, N.; Patra, A.; Chakravarty, M.; Saha, B. Engineering the reverse micellar-templated Co(OH)<sub>2</sub> nanospheres based Pickering emulsion and unveiling the mechanism of ambiguous phase separation. *J. Mol. Liq.* **2024**, *413*, 125904. [[CrossRef](#)]
34. Lindner, M.; Bäumlner, M.; Stäbler, A. Inter-Correlation among the Hydrophilic–Lipophilic Balance, Surfactant System, Viscosity, Particle Size, and Stability of Candelilla Wax-Based Dispersions. *Coatings* **2018**, *8*, 469. [[CrossRef](#)]
35. Chen, J.; He, L.; Luo, X.; Zhang, C. Foaming of crude oil: Effect of acidic components and saturation gas. *Colloids Surf. A Physicochem. Eng. Asp.* **2018**, *553*, 432–438. [[CrossRef](#)]
36. Shuttleworth, P.S.; Díez-Pascual, A.M.; Marco, C.; Ellis, G. Flexible Bionanocomposites from Epoxidized Hemp Seed Oil Thermosetting Resin Reinforced with Halloysite Nanotubes. *J. Phys. Chem. B* **2017**, *121*, 2454–2467. [[CrossRef](#)]
37. Marhamati, M.; Ranjbar, G.; Rezaie, M. Effects of emulsifiers on the physicochemical stability of Oil-in-water Nanoemulsions: A critical review. *J. Mol. Liq.* **2021**, *340*, 117218. [[CrossRef](#)]
38. Zhu, P.; Wang, F.; Ding, Y.; Zhang, S.; Gao, C.; Liu, P.; Yang, M. Double Phase Inversion of Pickering Emulsion Induced by Magnesium Hydroxide Nanosheets Adsorbed with Sodium Dodecyl Sulfate. *Langmuir* **2021**, *37*, 4082–4090. [[CrossRef](#)]
39. Koochakzadeh, A.; Teimouri, A.; Tohidi, E.; Ashrafizadeh, M.; Enzmann, F.; Kersten, M.; Sadeghnejad, S. Review on using pH-sensitive microgels as enhanced oil recovery and water shutoff agents: Concepts, recent developments, and future challenges. *Geoenergy Sci. Eng.* **2023**, *223*, 211477. [[CrossRef](#)]
40. Rahaman, S.M.; Joshi, D.; Patra, A.; Mandal, T.; Khatun, N.; Dhibar, S.; Saha, R.; Mandal, A.; Kumar, D.; Saha, B. A pH switchable Pickering emulsion stabilised by controlled non-conventional lanthanum sulfide nanoparticles, in situ hydrophobized with a cationic surfactant. *New J. Chem.* **2024**, *48*, 4063–4076. [[CrossRef](#)]
41. Chi, M.; Hu, J.; Wang, X.; He, R.; Wang, Z.; Li, S.; Hu, S.; Sun, S. Preparation and application of pH-Responsive and high salt-tolerant silica-based amphiphilic Janus nanosheets for enhanced heavy oil recovery. *Geoenergy Sci. Eng.* **2023**, *230*, 212210. [[CrossRef](#)]
42. Hua, X.; Bevan, M.A.; Frechette, J. Reversible Partitioning of Nanoparticles at an Oil–Water Interface. *Langmuir* **2016**, *32*, 11341–11352. [[CrossRef](#)] [[PubMed](#)]
43. Feng, X.; Dai, H.; Ma, L.; Fu, Y.; Yu, Y.; Zhou, H.; Guo, T.; Zhu, H.; Wang, H.; Zhang, Y. Properties of Pickering emulsion stabilized by food-grade gelatin nanoparticles: Influence of the nanoparticles concentration. *Colloids Surf. B Biointerfaces* **2020**, *196*, 111294. [[CrossRef](#)] [[PubMed](#)]
44. Xie, D.; Jiang, Y. The mediated rheological properties of emulsions stabilized by thread-like mesoporous silica nanoparticles in combination with CTAB. *Soft Matter* **2022**, *18*, 7782–7793. [[CrossRef](#)]
45. Etemad, S.; Kantzas, A.; Bryant, S. Efficient nanoparticle transport via CO<sub>2</sub> foam to stabilize oil in water emulsions. *Fuel* **2020**, *276*, 118063. [[CrossRef](#)]
46. Kumar, G.; Mani, E.; Sangwai, J.S. Impact of surface-modified silica nanoparticle and surfactant on the stability and rheology of oil-in-water Pickering and surfactant-stabilized emulsions under high-pressure and high-temperature. *J. Mol. Liq.* **2023**, *379*, 121620. [[CrossRef](#)]
47. Chen, X.; Xie, X.t.; Li, Y.; Chen, S. Investigation of the synergistic effect of alumina nanofluids and surfactant on oil recovery—Interfacial tension, emulsion stability and viscosity reduction of heavy oil. *Pet. Sci. Technol.* **2018**, *36*, 1131–1136. [[CrossRef](#)]
48. Mandal, T.; Rahaman, S.M.; Saha, B.; Khatun, N.; Patra, A.; Mukherjee, A.; Nandi, M.; Dhak, D.; Roy, S.; Saha, B. Comprehensive evaluation of non-conventional lanthanum phosphate nanospheres inside water-in-oil microemulsion scaffolds and their utilization in the assessment of surfactant-free TiO<sub>2</sub>-based Pickering emulsion formulations. *New J. Chem.* **2024**, *48*, 10112–10125. [[CrossRef](#)]

**Disclaimer/Publisher’s Note:** The statements, opinions and data contained in all publications are solely those of the individual author(s) and contributor(s) and not of MDPI and/or the editor(s). MDPI and/or the editor(s) disclaim responsibility for any injury to people or property resulting from any ideas, methods, instructions or products referred to in the content.